

## Low power consumption resistance random access memory with Pt/InOx/TiN structure

Jyun-Bao Yang, Ting-Chang Chang, Jheng-Jie Huang, Yu-Ting Chen, Hsueh-Chih Tseng, Ann-Kuo Chu, Simon M. Sze, and Ming-Jinn Tsai

Citation: [Applied Physics Letters](#) **103**, 102903 (2013); doi: 10.1063/1.4818672

View online: <http://dx.doi.org/10.1063/1.4818672>

View Table of Contents: <http://scitation.aip.org/content/aip/journal/apl/103/10?ver=pdfcov>

Published by the [AIP Publishing](#)

---

### Articles you may be interested in

[Stabilizing resistive switching performances of TiN/MgZnO/ZnO/Pt heterostructure memory devices by programming the proper compliance current](#)

Appl. Phys. Lett. **104**, 043508 (2014); 10.1063/1.4863744

[Mechanism of power consumption inhibitive multi-layer Zn:SiO<sub>2</sub>/SiO<sub>2</sub> structure resistance random access memory](#)

J. Appl. Phys. **114**, 234501 (2013); 10.1063/1.4843695

[Unipolar resistive switching behavior of Pt/Li x Zn1 x O/Pt resistive random access memory devices controlled by various defect types](#)

Appl. Phys. Lett. **101**, 203501 (2012); 10.1063/1.4766725

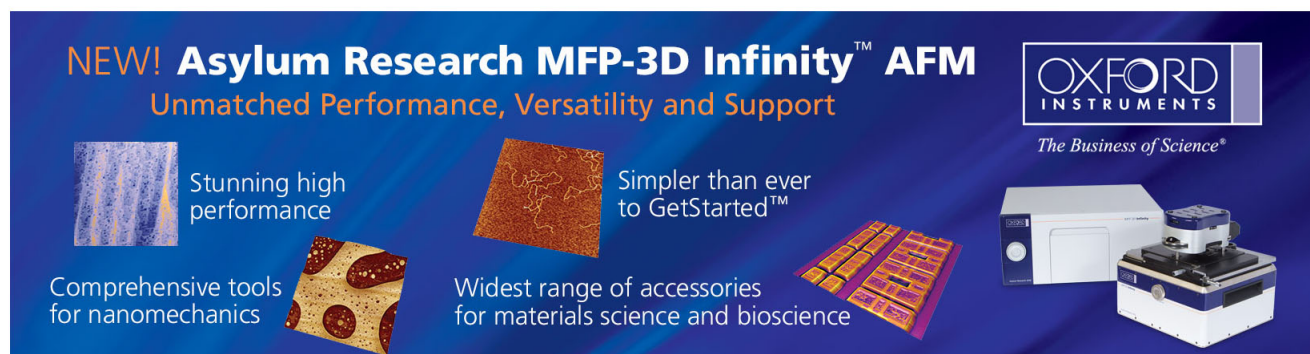
[Semiconducting-like filament formation in TiN/HfO<sub>2</sub>/TiN resistive switching random access memories](#)

Appl. Phys. Lett. **100**, 142102 (2012); 10.1063/1.3696672

[Low-power TiN/Al<sub>2</sub>O<sub>3</sub>/Pt resistive switching device with sub-20 A switching current and gradual resistance modulation](#)

J. Appl. Phys. **110**, 094104 (2011); 10.1063/1.3657938

---

The advertisement features a dark blue background with white and orange text. At the top left, it reads 'NEW! Asylum Research MFP-3D Infinity™ AFM' in large white letters, followed by 'Unmatched Performance, Versatility and Support' in orange. On the right, the Oxford Instruments logo is shown with the tagline 'The Business of Science®'. Below the text are four images: a blue textured surface, a brown textured surface, a yellow and red patterned surface, and a photograph of the MFP-3D Infinity AFM instrument. Each image is accompanied by a short text description: 'Stunning high performance', 'Simpler than ever to GetStarted™', 'Comprehensive tools for nanomechanics', and 'Widest range of accessories for materials science and bioscience'.

## Low power consumption resistance random access memory with Pt/InO<sub>x</sub>/TiN structure

Jyun-Bao Yang,<sup>1</sup> Ting-Chang Chang,<sup>1,2,3,a)</sup> Jheng-Jie Huang,<sup>2</sup> Yu-Ting Chen,<sup>1</sup> Hsueh-Chih Tseng,<sup>2</sup> Ann-Kuo Chu,<sup>1</sup> Simon M. Sze,<sup>2,4</sup> and Ming-Jinn Tsai<sup>5</sup>

<sup>1</sup>Department of Photonics, National Sun Yat-Sen University, Kaohsiung, Taiwan

<sup>2</sup>Department of Physics, National Sun Yat-Sen University, Kaohsiung, Taiwan

<sup>3</sup>Advanced Optoelectronics Technology Center, National Cheng Kung University, Taiwan

<sup>4</sup>Department of Electronics Engineering, National Chiao Tung University, Hsinchu, Taiwan

<sup>5</sup>Electronics and Optoelectronics Research Laboratory, Industrial Technology Research Institute, Chutung, Hsinchu, Taiwan

(Received 16 April 2013; accepted 29 July 2013; published online 4 September 2013)

In this study, the resistance switching characteristics of a resistive random access memory device with Pt/InO<sub>x</sub>/TiN structure is investigated. Unstable bipolar switching behavior is observed during the initial switching cycle, which then stabilizes after several switching cycles. Analyses indicate that the current conduction mechanism in the resistance state is dominated by Ohmic conduction. The decrease in electrical conductance can be attributed to the reduction of the cross-sectional area of the conduction path. Furthermore, the device exhibits low operation voltage and power consumption. © 2013 AIP Publishing LLC. [<http://dx.doi.org/10.1063/1.4818672>]

Due to the continuous miniaturization of device dimensions, floating-gate memory technology has reached its physical limits.<sup>1–3</sup> Resistive random access memory (RRAM) has been investigated to solve these problems due to its advantageous properties of simple structure, high density, and low power consumption.<sup>4–7</sup> The resistance switching (RS) characteristics have been studied in various materials such as organic materials,<sup>8</sup> perovskite oxides,<sup>9</sup> and binary metal oxides.<sup>10–14</sup> In this work, the RS behavior of a Pt/InO<sub>x</sub>/TiN device is investigated. Indium oxide (InO<sub>x</sub>) is chosen to be the RS layer because indium is widely used in applications of optoelectronic devices, such as indium-gallium-zinc-oxide (IGZO) thin film transistors.<sup>15–18</sup> It is notable that the RRAM device with Pt/InO<sub>x</sub>/TiN structure exhibits good properties of low power consumption and low operation voltage.

The 200 nm SiO<sub>2</sub> LTO (low temperature oxide) was deposited on the TiN/SiO<sub>2</sub>/Si substrate and the via hole (4 × 4 μm) was defined by etching the LTO layer. The 30 nm InO<sub>x</sub> film was deposited on the TiN by RF sputtering the In<sub>2</sub>O<sub>3</sub> target in Ar ambiance at room temperature. Subsequently, the top electrode (Pt) was deposited on the InO<sub>x</sub> film by DC sputtering and the Pt/InO<sub>x</sub>/TiN structure was completed, as shown in inset (ii) of Fig. 1. The RS characteristics for the Pt/InO<sub>x</sub>/TiN device were measured by an Agilent B1500 semiconductor parameter analyzer and a Cascade M150 probe station. During the measurement process, bias voltage was applied on the Pt electrode and the TiN electrode was grounded.

Figure 1 shows the current-voltage (I-V) curves of the Pt/InO<sub>x</sub>/TiN device with the characteristic exhibiting a bipolar RS behavior. The conduction paths are constructed during the forming process by applying a +10 V bias with a 100 μA current compliance, and the resistance state is at low

resistance state (LRS) after the forming process, as shown in inset (i) of Fig. 1. Subsequently, the resistance state can be switched from LRS to high resistance state (HRS) by the reset process sweeping voltage from 0 V to –1.3 V. After the reset process, the resistance state can be returned from HRS to LRS by sweeping voltage from 0 V to +1 V with a 1 mA current compliance (set process). The reset voltage is defined as the voltage where current starts to decrease during the reset process; likewise, the set voltage is defined as the voltage where the current increases abruptly during the set process.

The black line shows the switching behavior in transient mode (TM), which is obtained after the forming process. However, the RS behavior shows unstable characteristics during the initial switching cycles but tends to stabilize after several switching cycles. The stable RS behavior (in red) is labeled as steady mode (SM). Comparisons of I-V curves

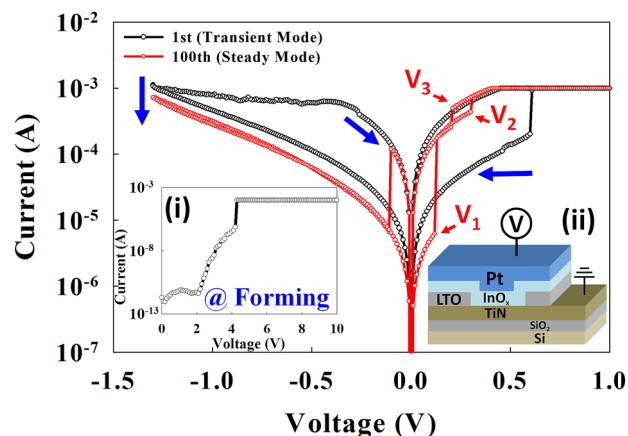


FIG. 1. The bipolar switching behavior of the Pt/InO<sub>x</sub>/TiN structure. The inset (i) is the forming process and inset (ii) is the Pt/InO<sub>x</sub>/TiN structure schematic diagram.

<sup>a)</sup>tcchang@mail.phys.nsysu.edu.tw.

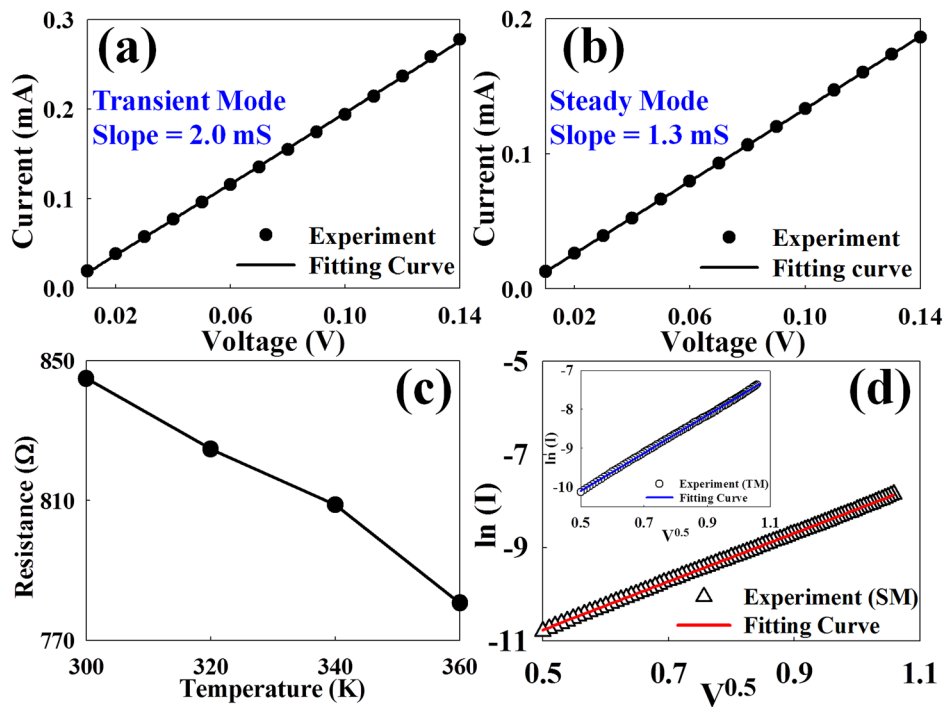


FIG. 2. The current conduction mechanism of LRS is Ohmic emission for (a) TM and (b) SM. (c) The resistance values of LRS for temperatures ranging from 300 K to 360 K. (d) the current conduction mechanism of HRS in SM and TM.

between TM and SM indicate that the set and reset voltages in SM are smaller than those in TM and the HRS current in SM is lower than that in TM, as indicated by blue arrows. The self-compliance behavior is observed in the current characteristic among the voltage ranges between  $V_1$  and  $V_2$  in the set process, as shown in Fig. 1.<sup>19</sup>

In order to investigate the carrier transport behavior of LRS and HRS, the current mechanisms are analyzed.<sup>20</sup> The result indicates that the current conduction of TM and SM are both dominated by Ohmic conduction in LRS, as shown in Figs. 2(a) and 2(b). The electrical conductance ( $G$ ) of LRS can be obtained from the slope of Ohmic fitting. The values of the slope are  $2.0 \times 10^{-3}$  and  $1.3 \times 10^{-3}$  for TM and SM, respectively, shown in Figs. 2(a) and 2(b). According to the electrical conductance equation:  $G = \frac{\sigma A_{CP}}{\ell}$ , the electrical conductance value of LRS decreases as  $A_{CP}$  decreases. The  $\sigma$ ,  $A_{CP}$ , and  $\ell$  are electric conductivity, cross-section area of conduction path, and length of conduction path, respectively. That the electrical conductance value for TM (2.0 mS) is larger than that for SM (1.3 mS) indicates that the cross-sectional area of the conduction path ( $A_{CP}$ ) in SM is smaller than in TM. Subsequently, the current conduction mechanisms of TM and SM are both dominated by Schottky emission in HRS, as shown in Fig. 2(d). When the device is switched to HRS, the thick insulation between conduction path and Pt electrode is formed. Hence, electrons require sufficient thermal energy to overcome the barrier. In addition, variations of resistance value at LRS are observed at various temperatures from 300 K to 360 K and are shown in Fig. 2(c). The resistance value of LRS decreases as temperature increases.<sup>21</sup>

Figure 3 shows the RS behavior mechanism. During the forming process, a high positive voltage is applied, and the conduction path of metal-like filament is formed because the In-O bonds are broken by energetic electrons and the oxygen ions migrate to the Pt electrode following the electric field

direction.<sup>23,24</sup> Large amount of oxygen ions are formed during the forming process because they cannot react with the Pt electrode. Hence, the variable series resistor (VSR) of indium oxide with high-concentration oxygen will be formed between the conduction path and Pt during the switching cycles,<sup>22</sup> and the oxygen ions can be stored in the VSR region, as shown in Fig. 3(a).

The  $A_{CP}$  in TM is larger than that in SM because the high forming voltage seriously damages the indium oxide

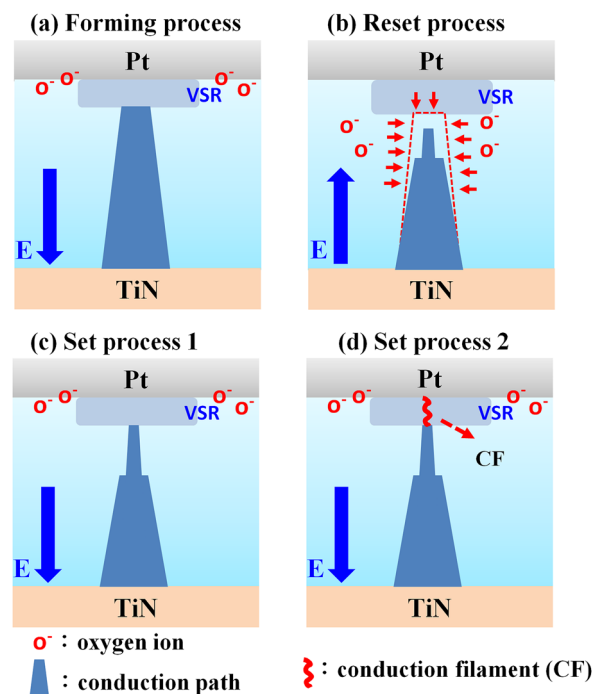


FIG. 3. The resistance switching mechanism of Pt/InO<sub>x</sub>/TiN structure during (a) forming process, (b) reset process in SM, with TM differences indicated by red dashed line; (c) set process 1 in SM, and (d) set process 2 in SM.

film and forms a thick conduction path. When a negative voltage is applied, the large number of oxygen ions is re-combined with the end of conduction path, as well as around the conduction path, as shown in Fig. 3(b). Hence, the  $A_{CP}$  will be reduced because of the oxidation around the conduction path, and the shape will become sharper after several DC switching cycles. A small  $A_{CP}$  induces serious local Joule heating effect generated by high current density, and this serious local Joule heating enhances the speed of oxidation. Accordingly, the current decreases abruptly during the reset process in SM.

Conversely, the conduction path is re-formed by applying a positive voltage due to the In-O bond breaking by energetic electrons. The set voltage in SM is smaller than that in TM because the smaller  $A_{CP}$  in SM induces a stronger electric field at the end of the conduction path and allows electrons break to the In-O bonds more easily. Furthermore, the current increases abruptly at  $V_1$  in the set process, and the self-compliance behavior occurs between  $V_1$  and  $V_2$  due to the formation of the VSR region, as shown in Fig. 3(c). As the applied voltage exceeds  $V_2$ , the current abruptly increases due to VSR breakage by the higher tip electric field and the resulting formation of a conduction filament (CF) in the VSR region, as shown in Fig. 3(d). Subsequently, while sweeping from +1.0 V back toward 0 V, the current decreases abruptly and the self-compliance behavior occurs at  $V_3$ . This is because that the CF in the VSR region is oxidized and destroyed by surrounding high-concentration oxygen ions. Furthermore, the reduced resistance value at higher temperatures in LRS shown, in Fig. 2(c), demonstrates that existence of the insulating VSR.

Figure 4 shows the I-V curves for different current compliances of 1 mA, 300  $\mu$ A, and 50  $\mu$ A. The LRS and HRS resistances are extracted at 0.1 V during 100 DC switching cycles, as shown in inset (i) and (ii) of Fig. 4. The resistance of LRS with low current compliance (LCC) is higher than that of high current compliance (HCC) since the  $A_{CP}$  is reduced as the current compliance decreases. The resistance of HRS increases with decreasing current compliance because the smaller  $A_{CP}$  in LCC induces higher Joule heating effect and enhances the oxidation reaction.

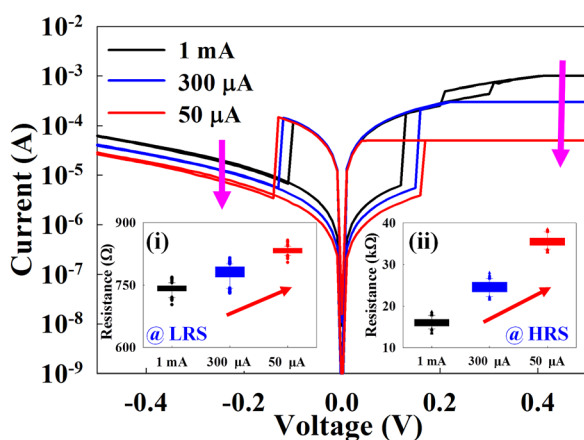


FIG. 4. I-V curves for different current compliances (1 mA, 300  $\mu$ A, and 50  $\mu$ A). The inset (i) and (ii) show resistance value of LRS and HRS for different current compliance.

In summary, the RRAM device with Pt/InO<sub>x</sub>/TiN structure exhibits bipolar RS behavior. The RS behavior is unstable during initial switching cycles and then tends to be stable after several more switching cycles. According to the analysis of LRS electrical conductance, the  $A_{CP}$  will be decreased during switching cycles. The stable RS behavior can be attributed to the set process stability brought about by enhancement of the tip electric field caused by reduced  $A_{CP}$ . In addition, the current in SM decreases abruptly during the reset process since the speed of the oxidation reaction is enhanced by the serious Joule heating effect which has been induced by the smaller  $A_{CP}$ . Hence, the smaller  $A_{CP}$  leads to a reduction of the set voltage and HRS current. The relationship between the resistance and  $A_{CP}$  can be further confirmed by varying the current compliance. The resistance values of LRS and HRS increase with decreasing current compliance owing to the reduction of the  $A_{CP}$ . Since power consumption is an important issue for portable electric product applications, the RRAM device in this study can achieve the low power consumption due to its low switching voltage and operating current characteristics.

This work was performed at National Science Council Core Facilities Laboratory for Nano-Science and Nano-Technology in Kaohsiung-Pingtung area, NSYSU Center for Nanoscience and Nanotechnology and was supported by the National Science Council of the Republic of China under Contract No. NSC-102-2120-M-110-001.

- <sup>1</sup>S. Tiwari, F. Rana, K. Chan, H. Hanafi, W. Chan, and D. Buchanan, *IEEE International Electron Devices Meeting 1995*, p. 521.
- <sup>2</sup>T. C. Chang, F. Y. Jian, S. C. Chen, and Y. T. Tsai, *Mater. Today* **14**, 608 (2011).
- <sup>3</sup>J. Lu, T. C. Chang, Y. T. Chen, J. J. Huang, P. C. Yang, S. C. Chen, H. C. Huang, D. S. Gan, N. J. Ho, Y. Shi, and A. K. Chu, *Appl. Phys. Lett.* **96**, 262107 (2010).
- <sup>4</sup>K. M. Kim, B. J. Choi, S. J. Song, G. H. Kim, and C. S. Hwang, *J. Electrochem. Soc.* **156**, G213 (2009).
- <sup>5</sup>J. Huang, T. C. Chang, J. B. Yang, S. C. Chen, P. C. Yang, Y. T. Chen, H. C. Tseng, S. M. Sze, A. K. Chu, and M. J. Tsai, *IEEE Electron Device Lett.* **33**, 1387 (2012).
- <sup>6</sup>Y. E. Syu, T. C. Chang, T. M. Tsai, Y. C. Hung, K. C. Chang, M. J. Tsai, M. J. Kao, and S. M. Sze, *IEEE Electron Device Lett.* **32**, 545 (2011).
- <sup>7</sup>H. Shima, F. Takano, H. Muramatsu, H. Akinaga, I. H. Inoue, and H. Takagi, *Appl. Phys. Lett.* **92**, 043510 (2008).
- <sup>8</sup>L. P. Ma, J. Liu, and Y. Yang, *Appl. Phys. Lett.* **80**, 2997 (2002).
- <sup>9</sup>T. Fujii, M. Kawasaki, A. Sawa, H. Akoh, Y. Kawazoe, and Y. Tokura, *Appl. Phys. Lett.* **86**, 012107 (2005).
- <sup>10</sup>Y. T. Chen, T. C. Chang, J. J. Huang, H. C. Tseng, P. C. Yang, A. K. Chu, J. B. Yang, H. C. Huang, D. S. Gan, M. J. Tsai, and S. M. Sze, *Appl. Phys. Lett.* **102**, 043508 (2013).
- <sup>11</sup>L. W. Feng, C. Y. Chang, Y. F. Chang, W. R. Chen, S. Y. Wang, P. W. Chiang, and T. C. Chang, *Appl. Phys. Lett.* **96**, 052111 (2010).
- <sup>12</sup>L. W. Feng, C. Y. Chang, Y. F. Chang, T. C. Chang, S. Y. Wang, S. C. Chen, C. C. Lin, S. C. Chen, and P. W. Chiang, *Appl. Phys. Lett.* **96**, 222108 (2010).
- <sup>13</sup>A. Sawa, *Mater. Today* **11**, 28 (2008).
- <sup>14</sup>H. Y. Lee, P. S. Chen, T. Y. Wu, C. C. Wang, P. J. Tzeng, C. H. Lin, F. Chen, M. J. Tsai, and C. Lien, *Appl. Phys. Lett.* **92**, 142911 (2008).
- <sup>15</sup>G. Goncalves, P. Barquinha, L. Pereira, N. Franco, E. Alves, R. Martins, and E. Fortunato, *Electrochem. Solid-State Lett.* **13**, H20 (2010).
- <sup>16</sup>T. C. Chen, T. C. Chang, C. T. Tsai, T. Y. Hsieh, S. C. Chen, C. S. Lin, M. C. Hung, C. H. Tu, J. J. Chang, and P. L. Chen, *Appl. Phys. Lett.* **97**, 112104 (2010).
- <sup>17</sup>C. T. Tsai, T. C. Chang, S. C. Chen, I. Lo, S. W. Tsao, M. C. Hung, J. J. Chang, C. Y. Wu, and C. Y. Huang, *Appl. Phys. Lett.* **96**, 242105 (2010).
- <sup>18</sup>M. C. Chen, T. C. Chang, C. T. Tsai, S. Y. Huang, S. C. Chen, C. W. Hu, S. M. Sze, and M. J. Tsai, *Appl. Phys. Lett.* **96**, 262110 (2010).

- <sup>19</sup>C. B. Lee, D. S. Lee, A. Benayad, S. R. Lee, M. Chang, M. J. Lee, J. Hur, Y. B. Kim, C. J. Kim, and U. I. Chung, *IEEE Electron Device Lett.* **32**, 399 (2011).
- <sup>20</sup>S. M. Sze and K. K. Ng, *Physics of Semiconductor Devices*, 3rd ed. (Wiley-Interscience, 2006).
- <sup>21</sup>H. C. Tseng, T. C. Chang, J. J. Huang, P. C. Yang, Y. T. Chen, F. Y. Jian, S. M. Sze, and M. J. Tsai, *Appl. Phys. Lett.* **99**, 132104 (2011).
- <sup>22</sup>W. Banerjee, S. Maikap, C. S. Lai, Y. Y. Chen, T. C. Tien, H. Y. Lee, W. S. Chen, F. T. Chen, M. J. Kao, M. J. Tsai, and J. R. Yang, *Nanoscale Research Lett.* **7**, 194 (2012).
- <sup>23</sup>C. Y. Lin, C. Y. Wu, C. Y. Wu, C. Hu, and T. Y. Tseng, *J. Electrochem. Soc.* **154**, G189 (2007).
- <sup>24</sup>X. Gao, Y. Xia, J. Ji, H. Xu, Y. Su, H. Li, C. Yang, H. Guo, J. Yin, and Z. Liu, *Appl. Phys. Lett.* **97**, 193501 (2010).